Cogn Neurodyn (2011) 5:1–12
DOI 10.1007/s11571-010-9130-0

RESEARCH ARTICLE

# Transitory behaviors in diffusively coupled nonlinear oscillators

**Satoru Tadokoro · Yutaka Yamaguti · Hiroshi Fujii · Ichiro Tsuda**

Received: 16 May 2010 / Revised: 8 August 2010 / Accepted: 12 August 2010 / Published online: 20 January 2011


**Abstract** We study collective behaviors of diffusively coupled oscillators which exhibit out-of-phase synchrony for the case of weakly interacting two oscillators. In large populations of such oscillators interacting via one-dimensionally nearest neighbor couplings, there appear various collective behaviors depending on the coupling strength, regardless of the number of oscillators. Among others, we focus on an intermittent behavior consisting of the all-synchronized state, a weakly chaotic state and some sorts of metachronal waves. Here, a metachronal wave means a wave with orderly phase shifts of oscillations. Such phase shifts are produced by the dephasing interaction which produces the out-of-phase synchronized states in two coupled oscillators. We also show that the abovementioned intermittent behavior can be interpreted as in-out intermittency where two saddles on an invariant subspace, the all-synchronized state and one of the metachronal waves play an important role.

**Keywords** Diffusively coupled systems of oscillators · Out-of-phase synchrony · Metachronal waves · In-out intermittency

S. Tadokoro (✉) · Y. Yamaguti · I. Tsuda
Laboratory of Computational Life Science, Research Institute of Electronic Science, Hokkaido University, Sapporo 060-0812, Japan
e-mail: tadokoro@math.sci.hokudai.ac.jp

H. Fujii
Department of Information and Communication Sciences, Kyoto Sangyo University, Kyoto 603-8555, Japan

I. Tsuda
Department of Mathematics, Graduate School of Science, Hokkaido University, Sapporo 060-0810, Japan

## Introduction

Electrically coupled interneurons via gap junctions (GJ) have been widely observed in the mammalian neocortex (Galarreta and Hestrin 1999; Gibson et al. 1999). Motivated by this observation, many theoretical studies of collective behaviors of GJ-coupled interneurons have been conducted by the use of neural oscillators interacting via diffusion type couplings.

Although it had been widely believed that the GJ-coupling among interneurons promotes their synchronous firing (Galarreta and Hestrin 1999; Gibson et al. 1999), Sherman and Rinzel (1992) first observed that weak GJ-coupling can lead dephasing and phase locking by anti-phase in two coupled neural oscillators. Later, Han et al. (1995, 1997) demonstrated how diffusion type weak couplings can lead to dephasing of two oscillators by using the Morris-Lecar model. They also found alternations between synchronization and desynchronization of oscillations in a large population of coupled oscillators. Also in other systems, for instance, in electrochemical dynamical systems, Karantonis and Nakabayashi (2001) found a similar phenomenon in diffusively coupled electrochemical oscillators. The present authors also found that some kinds of neural oscillator, when diffusively coupled, exhibit transitory behaviors, i.e., spontaneously irregular transitions between various dynamical states such as synchronized states and chaotic states (Tsuda et al. 2004).

The earlier studies mentioned above (Sherman and Rinzel 1992; Han et al. 1995, 1997; Karantonis and Nakabayashi 2001) and our previous study (Tsuda et al. 2004) show different synchronies in two-oscillator system with weak diffusion coupling. While two oscillators synchronize in anti-phase in the former cases, they

synchronize in out-of-phase indicating the phase difference not necessarily equal to $\pi$ in the latter. Little is known about collective behaviors in large populations of coupled oscillators which have the out-of-phase synchrony in the case of the two oscillator system. In this paper, we show that there appear various transitory behaviors in such diffusively coupled oscillators and one of them can be interpreted as in-out intermittency.

Transitory behaviors with aperiodic changes between dynamic states have been observed as cortical activity, such as fluctuations of local field potentials accompanying with transient synchrony (Gray et al. 1992) and spontaneous cortical activity which encompasses a set of dynamically switching cortical states (Kenet et al. 2003). Two of the present authors have proposed a hypothesis on the mechanism of the observed chaotic field (Fujii and Tsuda 2004), that the origin of temporal fluctuations and transient synchrony observed in the neocortical activity stems from chaotic transitions among dynamic states appearing in gap junction (GJ)-coupled interneuron systems. The GJ-coupled interneurons to pyramidal cells can influence in the fluctuations of membrane potentials of the pyramidal cells, which could be experimentally observed.

This paper is organized as follows: In section "A nonlinear oscillator model, its diffusively coupled system, and dynamics of diffusively coupled two oscillator system", we describe the nonlinear oscillator and its diffusively coupled system which we treat here. We also discuss the stability of synchronous states in diffusively coupled two oscillators. In section "Dynamics of diffusively coupled $N$-oscillator system", we discuss behaviors appearing in diffusively coupled $N$-oscillator system in the case of $N > 2$. In subsection "Bifurcation structures of periodic states and system size dependence", we discuss bifurcation structures of periodic states of coupled $N$-oscillator systems. And we also show that they, when viewed as functions of rescaled coupling strength $g/N^2$, are not depend on $N$ in the case of slightly large $N$. In subsection "Transitory behaviors", we discuss one of typical transitory behaviors appearing in the coupled systems. We also show that it can be interpreted as in-out intermittency. In subsection "Markov chain model", we calculate the probability distribution of laminar duration of the in-out intermittency and compare it with the one calculated by using a Markov chain model of the in-out-intermittency. In subsection "Bifurcations along with variation in the coupling strength", we describe various behaviors appearing through successive bifurcations with variations in the coupling strength. Section "Summary and discussion" is devoted to summary and discussion.

## A nonlinear oscillator model, its diffusively coupled system, and dynamics of diffusively coupled two oscillator system

### A nonlinear oscillator model and its diffusively coupled system

The nonlinear oscillator treated here is described by (Tsuda et al. 2004)

$$\begin{cases} \dfrac{dV}{dt} = -R - \mu V^2\left(V - \dfrac{3}{2}\right) + I \\ \dfrac{dR}{dt} = -R + \mu V^2 \end{cases} \tag{1}$$

When it is viewed as a neuron model, the variable $V$ represents the membrane potential of a neuron and the other variable $R$ is a recovery variable representing an activation state, and the parameter $I$ represents an injected current. This model has another parameter $\mu$ which will be fixed to the value, 1.65 throughout this article. Although this model is essentially the same as the Hindmarsh-Rose model (Hindmarsh and Rose 1984) with two variables, it was derived as a minimal one-parameter family of two-dimensional neural dynamical systems showing both Hopf bifurcation and saddle-node bifurcation (Tsuda et al. 2004). We called it $\mu$-model.

Figure 1a shows the bifurcation diagram of the model when the injected current $I$ is a bifurcation parameter. The model exhibits saddle-node bifurcation ($I = 0$) and Hopf bifurcation ($I \sim 0.19$), and there appears a limit cycle oscillation between these bifurcation points. Figure 1b shows nullclines for $V$ and $R$ together with a limit cycle for $I = 0.004$.

The diffusively coupled system of the $\mu$-models obeys the following equations:

$$\begin{cases} \frac{dV_i}{dt} &= -R_i - \mu V_i^2(V_i - \frac{3}{2}) + I + J_i \\ \frac{dR_i}{dt} &= -R_i + \mu V_i^2 \end{cases} \tag{2}$$

$$J_i = \begin{cases} g(V_2 - V_1) & (i = 1) \\ g(V_{i+1} + V_{i-1} - 2V_i) & (i = 2, ....., N-1) \\ g(V_{N-1} - V_N) & (i = N) \end{cases} \tag{3}$$

where $N$ is the number of oscillators and $g$ is the coupling strength. Here the couplings are introduced in variables $V_i$. We treat the case of one-dimensional nearest neighbor coupling with a free boundary condition, which is in accord with the Neumann type of boundary condition in the continuous space limit.

### A coupled two oscillator system

Before showing cases of large numbers of oscillators, in this subsection we treat the case of $N = 2$. In the weak interaction limit, the evolution of the phase difference

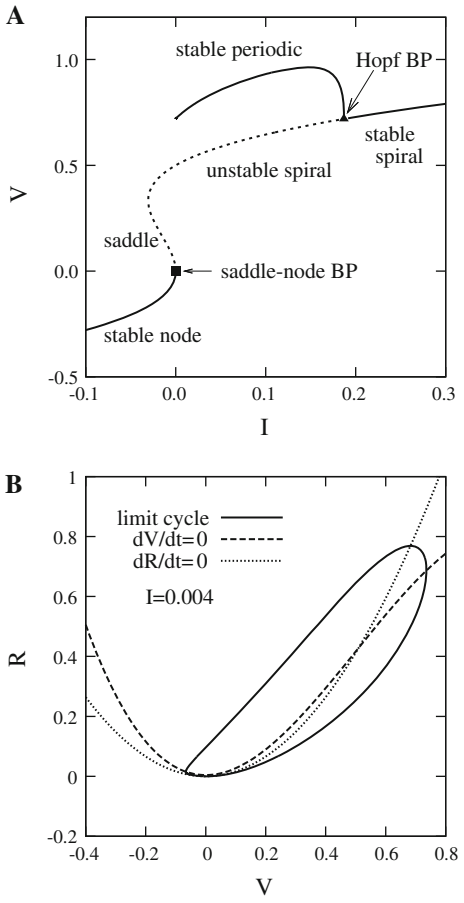


**Fig. 1** **a** Bifurcation diagram for a single $\mu$-model showing $V$ as a function of $I$. $\mu = 1.65$. For stable periodic states, maximum values of $V$ are plotted. **b** Nullclines for $V$ and $R$ together with a limit cycle. $I = 0.004$

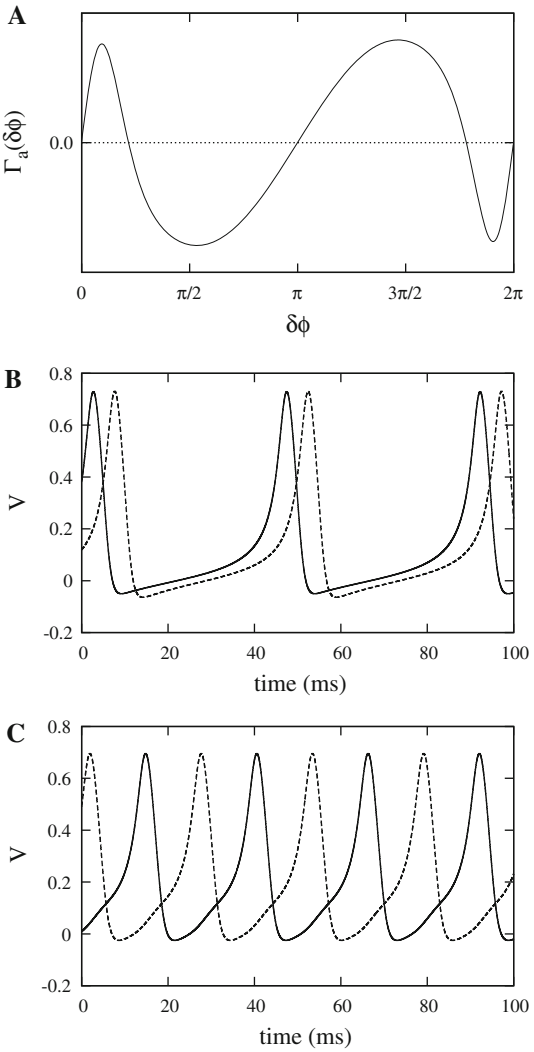


**Fig. 2** **a** Antisymmetric part of effective coupling, $\Gamma_a(\delta\phi)$. $I = 0.004$. **b** Time-series of $V_1$ and $V_2$ in an out-of-phase synchronized state of two interacting oscillators for $g = 0.005$. **c** Time-series of $V_1$ and $V_2$ in the anti-phase synchronized state for $g = 0.02$

$\delta\phi = \phi_1 - \phi_2$ between two oscillators with phases $\phi_1$ and $\phi_2$ is governed by (Kuramoto 1984)

$$\frac{\partial}{\partial t}\delta\phi = \Gamma_a(\delta\phi) \tag{4}$$

where $\Gamma_a$ is the antisymmetric part of the effective coupling defined by

$$\Gamma_a(\delta\phi) = \frac{1}{2\pi}\int_0^{2\pi} Z(\phi'+\delta\phi)(V(\phi'+\delta\phi) - V(\phi'))d\phi'. \tag{5}$$

Here $V(\phi')$ denotes the variable $V$ at phase $\phi'$ on the limit cycle. The phase sensitivity function $Z(\phi)$ gives the change of phase along the limit cycle caused by the change of state vector $(V, R)$ in phase space.

Figure 2a shows $\Gamma_a(\delta\phi)$ for $I = 0.004$. In this figure, it is shown that the system has three types of synchronized states: the unstable in-phase and anti-phase states, and the stable out-of-phase states. The time-series of $V_1$ and $V_2$ in one of the out-of-phase synchronized states for $I = 0.004$ and $g = 0.005$ is shown in Fig. 2b.

In the case of coexistence of a limit cycle and a stable node with an intervening saddle, it was shown that the saddle causes the deformations of the phase flow and thus the diffusion type of coupling between such oscillators can produce dephasing interaction under a certain condition (Han et al. 1995). In the case of the $\mu$-model, a limit cycle does not coexist with a saddle and a stable node (see Fig. 1). Nevertheless, such dephasing interaction can survive even after the saddle disappears via saddle-node bifurcation, because the main features of the phase flow in the vicinity of the limit cycle continue to remain unchanged (Han et al. 1995). Therefore, it is probable that the dephasing interaction in the case of the $\mu$-model is also attributed to this mechanism.

In the case of relatively strong coupling, where the discussion based on the effective coupling cannot be applicable, in-phase and anti-phase synchronization can be

stabilized, and either of them appears depending on the initial phase difference of two oscillators. The time-series of $V_1$ and $V_2$ in the anti-phase synchronized state for $g = 0.02$ is shown in Fig. 2c.

## Dynamics of diffusively coupled *N*-oscillator system

### Bifurcation structures of periodic states and system size dependence

In this subsection, we discuss bifurcation structures of periodic states of coupled *N*-oscillator systems, and show that they are almost independent of $N$ when viewed as function of rescaled coupling strength $g/N^2$, in the case of relatively large $N$.

In the continuous space limit, the coupling term of Eq. 3, $g(V_{i+1} + V_{i-1} - 2V_i)$ should be equivalent to $D\,\partial^2 V/\partial x^2$, where $x$ is a space variable. The coefficient $D$ is a diffusion coefficient defined by $g/N^2$ as $N \to \infty$ and $g \to \infty$, keeping $g/N^2$ constant. Thus, we expect that two systems with sufficiently large numbers of oscillators $N_1$ and $N_2$ ($\neq N_1$) exhibit the same behaviors at $g_1$ and $g_2$, respectively, if their rescaled coupling strengths are equal each other:

$$\frac{g_1}{N_1^2} \sim \frac{g_2}{N_2^2}. \tag{6}$$

Since this continuous limit is not mathematically straightforward, the scaling relation should be restricted to a certain range of finite system size. To demonstrate whether this scaling is realized or not, we study the bifurcation structures of periodic states of the coupled *N*-oscillator system for different $N$ viewing the (rescaled) coupling strength $g$ ($g/N^2$) as a bifurcation parameter.

Figure 3a–c show bifurcation structures in the case of $N = 8$, 16 and 17, respectively. The strength of $g$ ($g/N^2$) is shown on the lower (upper) abscissa. To follow the branching of solutions, we use AUTO (Doedel et al. 2002), a software for continuation and bifurcation problems. It is clear from Fig. 3a–c that the bifurcation structures, when viewing $g/N^2$ as a bifurcation parameter, are almost independent of $N$, except in the case that $g/N^2$ is very small.

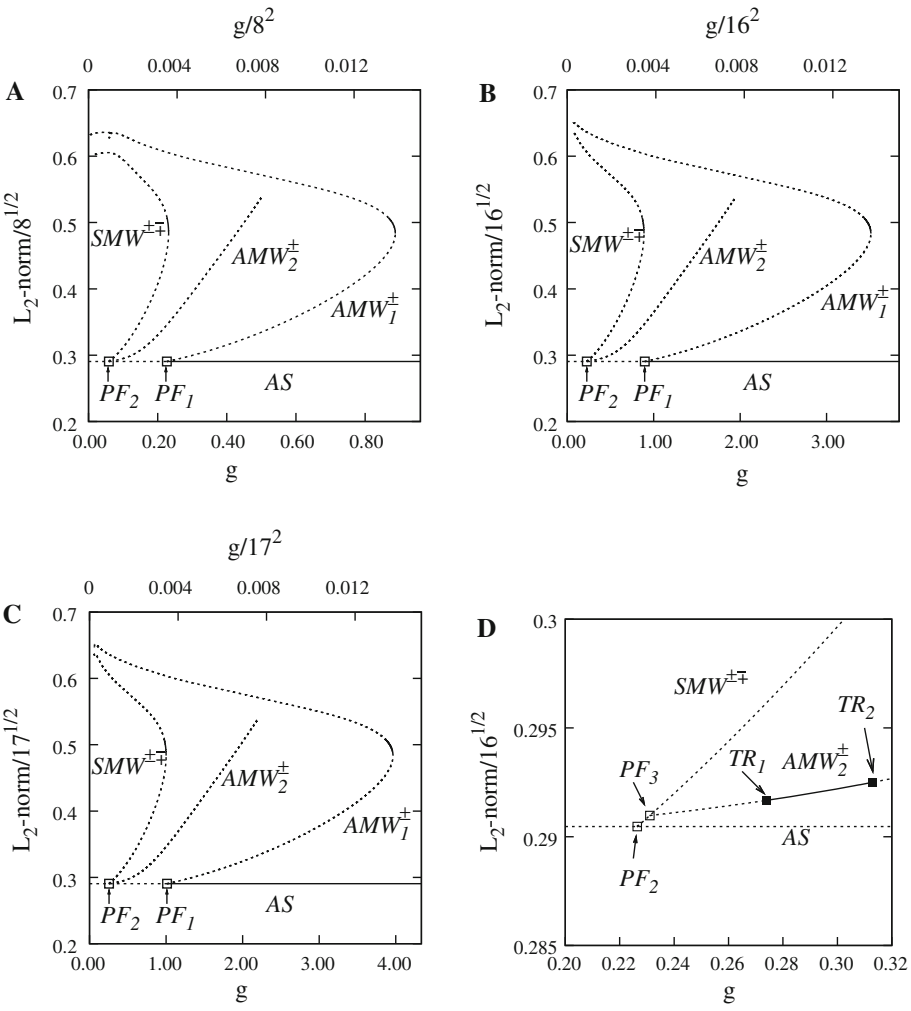


**Fig. 3** Bifurcation diagrams of periodic states of $N$ oscillators interacting diffusively via one-dimensional nearest-neighbor coupling. The (rescaled) coupling strength $g$ ($g/N^2$) is viewed as a bifurcation parameter, and is shown on the lower (higher) abscissas. The axis of the ordinate is for the $L_2$-norm divided by $\sqrt{N}$. Branches located at $g$ close to 0 which are not important for the discussion in this article are omitted. Stable and unstable branches are represented by *solid* and *dashed lines*, respectively. The branch of the all-synchronized state is marked with *AS*. The branches of out-of-phase synchronized state are marked with $SMW^{\pm\mp}$, $AMW_1^{\pm}$ and $AMW_2^{\pm}$. Branching points marked with $PF_1$, $PF_2$ and $PF_3$ are subcritical pitchfork bifurcation points. **a** $N = 8$. **b** $N = 16$. **c** $N = 17$. **d** Enlarged view of **b** near the branching point $PF_2$. Branching points marked with $TR_1$ and $TR_2$ are torus bifurcation points

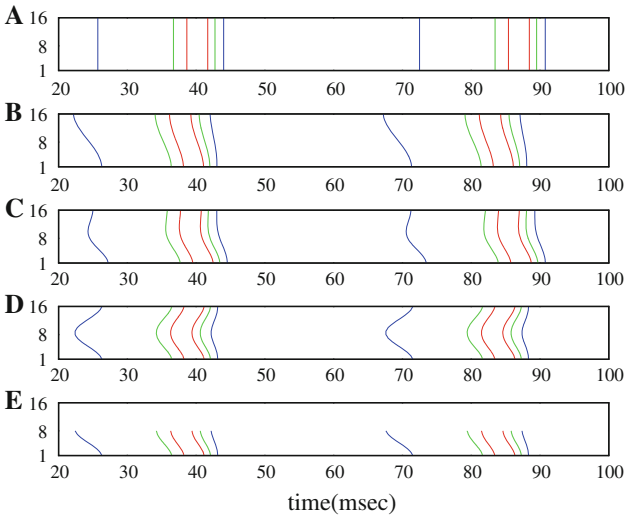


**Fig. 4** The contour plots of $V_i$ time-series of periodic states on the branches shown in Fig. 3. The vertical and horizontal directions indicate the oscillators' indices and time, respectively. *Red*, *green*, and *blue curves* are isopotential lines of $V_i = 0.55$, $V_i = 0.3$, and $V_i = 0.05$, respectively. Patterns are depicted during the period of two cycle. **a** $N = 16$. The states on the *AS* branch. **b** $N = 16$. The $AMW_1^+$ state at $g = 1.02$ ($g/N^2 \approx 0.003984$) and rescaled $L_2$-norm of 0.29. **c** $N = 16$. The $AMW_2^+$ state at $g = 0.255$ and rescaled $L_2$-norm of 0.2913. **d** $N = 16$. The $SMW^{+-}$ state at $g = 0.255$ and rescaled $L_2$-norm of 0.2937. **e** $N = 8$. The $AMW_1^+$ at $g = 0.255$ ($g/N^2 \approx 0.003984$) and rescaled $L_2$-norm of 0.2937. (Color figure online)

The horizontal straight line marked with *AS* in Fig. 3 represents the branch of the all-synchronized state in which all the oscillators are in-phase synchronized and are just on the unperturbed limit cycle orbit. The spatio-temporal contour maps of the amplitude of *V*-variables of a state on the *AS* branch in the case of $N = 16$ is shown in Fig. 4a.

Three curves marked with $AMW_{1,}^{\pm}$ $AMW_2^{\pm}$ and $SMW^{\pm\mp}$ in Fig. 3 represents out-of-phase synchronous branches on which oscillators are synchronized in out-of-phase. They arise due to the dephasing interaction that allows out-of-phase synchronous states in the case of $N = 2$. The states on these branches exhibit spatio-temporal patterns of metachronal waves because of their orderly phase shifts in oscillators' indices. Examples of such metachronal wave patterns are shown in Fig. 4b–e. These metachronal wave patterns can be classified into mirror asymmetric ones or symmetric ones with respect to oscillators indices. Thus we term these out-of-phase synchronous branches "asymmetric metachronal wave" ($AMW_{1,2}^{\pm}$) branches or "symmetric metachronal wave" ($SMW^{\pm\mp}$) branches. In fact, each of $AMW_1^{\pm}$, $AMW_2^{\pm}$ and $SMW^{\pm\mp}$ curves in Fig. 3 does not represent one branch but a pair of branches which is degenerated in $L_2$-norm. For instance the $SMW^{\pm\mp}$ curve corresponds to a pair of branches, $SMW^{+-}$ and $SMW^{-+}$. The superscripts such as "+" and "+−" of the labels are for distinction between paired branches. The essential difference between the paired branches is in the direction of phase shift with respect to oscillators' indices.

Since only lower half parts of these out-of-phase synchronous branches, that is, the parts rescaled $L_2$-norms of which are less than about 0.48 are important in the present study, hereafter when we say, for example, $AMW_1^{\pm}$ branch, it means its lower half part. We call a state on the $AMW_1^+$ branch, etc., simply a $AMW_1^+$ state, etc.

Figure 4b–d show spatio-temporal patterns of $AMW_1^+$, $AMW_2^+$, and $SMW^{+-}$ states, respectively, in the case of $N = 16$. The $AMW_1^-$, that are paired with the $AMW_1^+$ state exhibits the same pattern shown in Fig. 4b, except that the pattern is turned upside down. The same thing holds for the relation between the $AMW_2^+$ and $AMW_2^-$ states. The spatio-temporal pattern of $SMW^{-+}$ state, that is paired with the $SMW^{+-}$ state, is the same as the one shown in Fig. 4d, except that the upper and lower half parts are interchanged.

The scaling mentioned above appears also in the relation between the spatio-temporal patterns shown in Fig. 4b, e. The former figure shows the pattern of the $AMW_1^+$ state at $g/N^2 \approx 0.00398$ ($g = 1.02$) in the case of $N = 16$, and the latter shows the pattern of the $AMW_1^+$ state at the same $g/N^2$ ($g = 0.255$) in the case of $N = 8$. The latter pattern ($N = 8$) become almost the same as the former ($N = 16$) except that the vertical scale of the former is doubled.

It should be noted that the $SMW^{\pm\mp}$ branches in the case of $N = 16$ and $AMW_1^{\pm}$ branches in the case of $N = 8$ appear at the same position when measured in $g$ (not $g/N^2$) (see Fig. 3a, b). It should be also noted that the lower half part of the spatio-temporal pattern of the $SMW^{+-}$ state at $g = 0.255$ in the case of $N = 16$ (Fig. 4d) is the same as the one of the $AMW_1^+$ (Fig. 4e) state at the same $g$ in the case of $N = 8$. The same thing holds for the relation between the upper half part in the case of $N = 16$ and the pattern of the $AMW_1^-$ in the case of $N = 8$. In the case of even $N \geq 4$, a $SMW^{\pm\mp}$ state at certain $g$ for $N$ is composed of a pair of states $AMW_1^+$ and $AMW_1^-$ for $N/2$ at the same $g$, satisfying the mirror symmetry as a whole. Even in the case that $N(\geq 5)$ is odd, the same relation between a $SMW^{\pm\mp}$ state for $N$ and $AMW_1^{\pm}$ states for $(N-1)/2$ is effectively satisfied for relatively large $N$.

The reason why this hierarchical structure arises is as follows. The coupled systems discussed here have an invariant subspace due to the mirror symmetry with respect to the reverse of oscillators' indices. This mirror symmetric invariant subspace is defined by:

$$\left\{(V_1,..V_N,R_1,..R_N)|V_i=V_{N-i+1},R_i=R_{N-i+1}:i=1,...,\left\lfloor\frac{N}{2}\right\rfloor\right\}. \quad (7)$$

The $SMW^{\pm\mp}$ states are inside the invariant subspace. In the case of even $N$, within the invariant subspace, since the interaction between $N/2$-th oscillator and $N/2+1$-th one disappears, a coupled $N$-oscillator system can be decomposed into two identical coupled $N/2$-oscillator systems each of which obeys the free boundary condition. Thus if there exist a pair of out-of-synchronous states, for example, $AMW_1^{\pm}$ in the case of $N/2$, there should exist, in the case of $N$, a pair of states each of which is composed of the paired states for $N/2$ satisfying the mirror symmetry. In the case of odd $N$, a coupled $N$-oscillator system within the invariant subspace can be considered to consist of two identical coupled $(N-1)/2$-oscillator systems and one oscillator which locates between them. The analyses using AUTO suggest that in a $SMW^{+-}$ state, the trajectory of the centermost oscillator is approximately the same as its neighbor oscillators, i.e., $(N-1)/2$-th and $(N+1)/2$-th oscillators for relatively large $N$. Then the interactions between the centermost oscillator and the subsystems consisting of $(N-1)/2$ oscillators are approximately zero. Thus a coupled $N$-oscillator system in a $SMW^{\pm\mp}$ state can be effectively considered to consist of two identical coupled $(N-1)/2$-oscillator systems with the free boundary condition.

Now, let us pay attention to the normal and tangential stabilities of the $AS$ and $SMW^{+-}$ branches with respect to the invariant subspace, that play important roles in transitory behaviors discussed in the next subsection. While the $AS$ branch is stable at large $g/N^2$, it is unstable below $g/N^2 \sim 0.0035$. It is plausible to think that this $g$-dependence originates from the fact that the in-phase synchronized state in two interacting oscillators is unstable in the case of weak couplings and stable in the case of relatively strong couplings ("A nonlinear oscillator model, its diffusively coupled system, and dynamics of diffusively coupled two oscillator system"). The dependence of the stability of the $AS$ branch and the aforementioned scaling produce a region of $g$ where it is unstable for $N$ and is stable for $N/2$. Thus, in such a region, the $AS$ state for $N$ is a saddle, which is unstable transversely to the mirror symmetric invariant subspace and stable within it (ones are urged to recall that a coupled $N$-oscillator system within the invariant subspace can be decomposed into two identical coupled $\lfloor \frac{N}{2} \rfloor$ oscillator systems with free boundary condition). According to analyses of Floquet multipliers by using AUTO, whereas the $SMW^{+-}$ branch is unstable inside the invariant subspace, it is stable in the normal direction to the invariant subspace. Thus, below $g/N^2 \sim 0.0035$, there exist two saddles, i.e., $AS$ and $SMW^{+-}$ states in the invariant subspace. In the next subsection, we show that trajectories between these saddles are formed and transitory behaviors which consist of the saddles as dynamic components appear.

## Transitory behaviors

Various transitory behaviors appear depending on the (rescaled) coupling strength. Figure 5 shows the spatio-temporal contour map of the amplitude of $V$-variables of one of such transitory behaviors. This is the case of $N = 16$, $I = 0.004$ and $g = 0.255$. The same behaviors as shown in this figure appear in the case of other $N(>10)$ because of the scaling mentioned in the previous subsection.

In Fig. 5, there appear the same patterns as shown in Fig. 4a, d. They are marked with $AS$ and $SMW^{+-}$. These states are unstable, but each of them has a stable direction. Thus they appear as dynamic components of this transitory behavior. The pattern $AS$, which is sustained for some time, is transformed into the pattern labeled $MAMW_2^+$ or the one labeled $MAMW_2^-$. The patterns $MAMW_2^{\pm}$, which we call *modulated asymmetric metachronal waves*, represent dephasing processes of oscillators. The difference between $MAMW_2^+$ and $MAMW_2^-$ are simply in the direction of phase shift with respect to oscillators' indices. The dynamic states $MAMW_2^{\pm}$ originate from quasiperiodic states bifurcating from the bifurcation point on the $AMW_2^{\pm}$ branches, which are marked with $TR_1$ in Fig. 3d. After the appearance of one of these dephasing processes, the coupled system reaches the $SMW^{+-}$ state. The mirror symmetric pattern labeled $MSMW^{+-}$ (*modulated symmetric metachronal wave*) or the one labeled $WCS$ follows after $SMW^{+-}$. The pattern $MSMW^{+-}$, in which phase shifts between neighboring oscillators become less with the passage of time, corresponds to the transitions from $SMW^{+-}$ to $AS$. The pattern $WCS$ corresponds to the other transition processes from $SMW^{+-}$ to $AS$. This pattern includes a slightly complex pattern unlike $MSMW^{+-}$. In certain regions of the coupling strength, a state exhibiting $WCS$ pattern exists as a stable attractor ("Bifurcations along with variation in the coupling strength") and its largest Lyapunov exponent become small but still positive. Thus we name this dynamic state *weakly chaotic state*.

To make clear essential structure of the transitory behavior, we take a Poincaré section by cutting the trajectory, a part of which has the spatio-temporal structure shown in Fig. 5, with a hyper-plane defined by (Tsuda et al. 2004)

$$\left\{ (V_1, .., V_N, R_1, ..., R_N) | \frac{1}{N} \sum_{i=1}^{N} V_i = C \right\}. \tag{8}$$

Figure 6a shows the projection to the $(V_1, V_8)$ plane of the Poincaré map. Here we set $C$ at 0.2. An attractor representing the transitory behaviors is clearly visible. Parts of the attractor are marked with the same labels as the ones used in Fig. 5. The saddle states $AS$ and $SMW^{+-}$ are

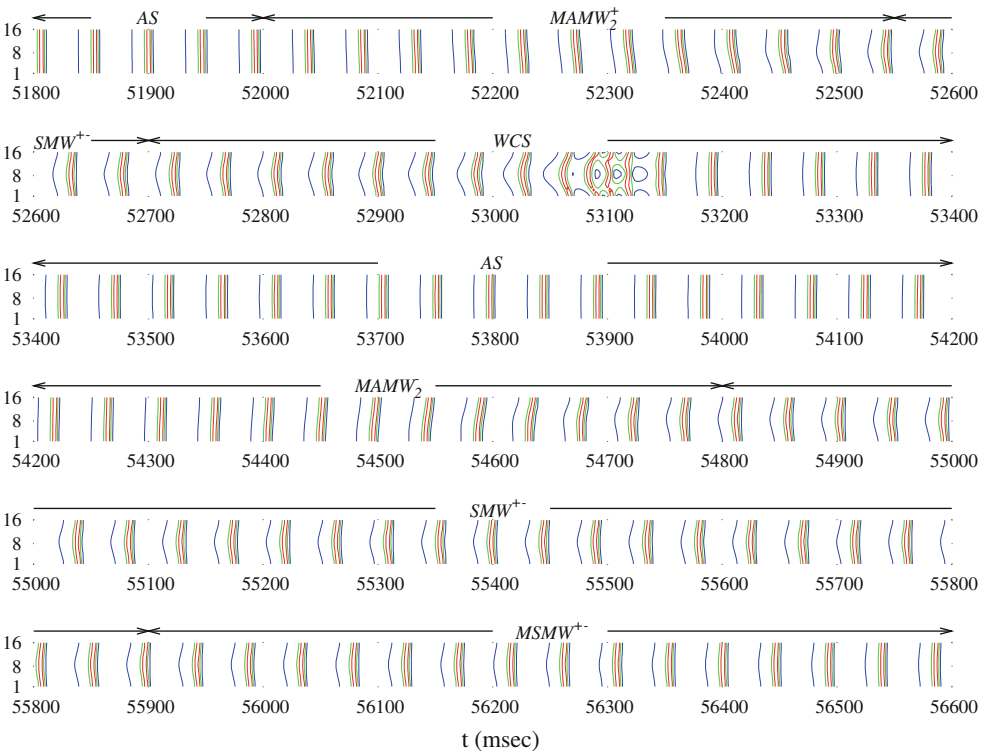


**Fig. 5** The contour plot of $V_i$ time-series in a typical transitory behavior exhibited by 16 coupled oscillators for $I = 0.004$ and $g = 0.255$. Initial conditions of $(V_i, R_i)$ are randomly chosen from the interval $(-0.2, 0.8)$. Characteristic patterns are marked with labels, *AS*, $SMW^{+-}$, $MSMW^{+-}$, and $MAMW_2^-$. Meanings of labels $MSMW^{+-}$ and $MAMW_2^-$ should be refer to the text

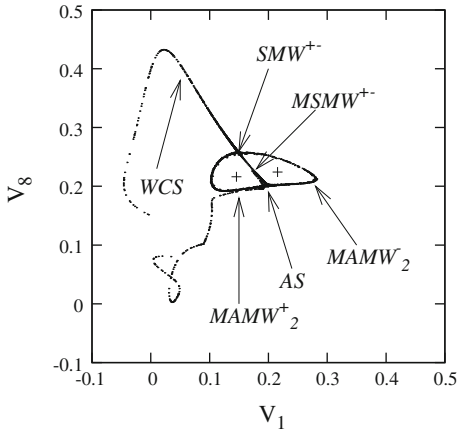


**Fig. 6** A Poincaré map for the transitory behavior shown in Fig. 5. The projection to the $(V_1, V_8)$ plane of the Poincaré map are shown. Correspondence between the parts of the attractor on the Poincaré section and the dynamic states appearing in Fig. 5 are shown by using the same labels used in Fig. 5. Positions of the unstable periodic states $AMW_2^{\pm}$ which are mentioned in the previous section are also indicated by the crosses

located at $(V_1, V_8) = (0.2, 0.2)$ and $\sim(0.15, 0.25)$, respectively. The transitional state $MAMW^+{}_2$ ($MAWM^-{}_2$) from *AS* to $SMW^{+-}$ state appears as the left (right) curve. The straight line-like path from $SMW^{+-}$ to *AS* represents the transitional state $MSMW^{+-}$. The other transitional state from $SMW^{+-}$ to *AS*, *WCS* appears as the twisted string.

We estimated the largest Lyapunov exponents of this attractor, using the standard method (Shimada and Nagashima 1979; Benettin et al. 1980a, b) and obtained $\lambda_1 = 1.537 \times 10^{-3}$. This indicate that the attractor is chaotic.

Figure 7a, b shows the time-series of distance of trajectories of the coupled oscillators from the mirror symmetric invariant subspace, which is mentioned in the previous subsection. One can see a characteristic of an intermittent behavior, that is, the existence of the trajectory intermittently approaching and leaving the invariant subspace. Figure 7c shows time-series of *V*-variables of the first and the eighth oscillators on the Poincaré section. The comparison between Fig. 7b, c makes clear that exponential increase and decrease in the distance with constant rates occur when $(V_1, V_8)$ is close to (0.2, 0.2) indicating *AS*, and close to around (0.15, 0.25) indicating $SMW^{+-}$, respectively. This intermittent behavior can be interpreted as in-out intermittency.

According to Ashwin, if the intersection of an attractor that exhibits intermittency with an invariant subspace is a minimal attractor, then the intermittency is called *on-off*. Otherwise, it is called *in-out* (Ashwin et al. 1999). The intersection of the attractor treated here with the invariant subspace is not a minimal attractor but contains at least two invariant sets, *AS* and $SMW^{+-}$, which cause the *out-phase* and the *in-phase*, respectively.

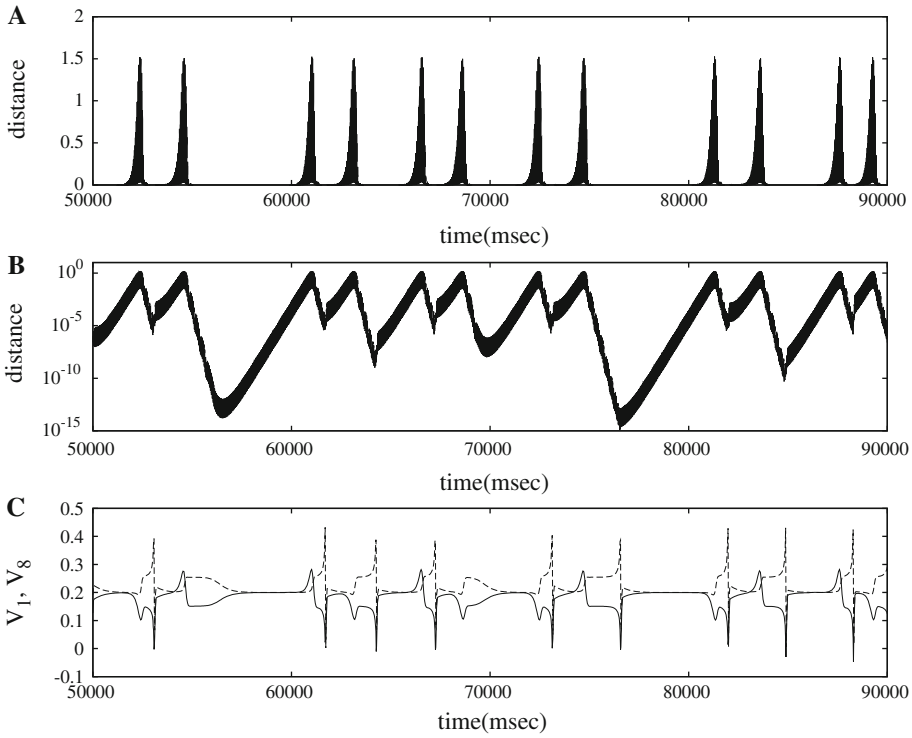


**Fig. 7** **a** Distance of the dynamical orbit in Fig. 6 from the mirror symmetric invariant subspace as a function of time in the linear scale. **b** The same plot as **a** but in a logarithmic scale. **c** The time-series of $V_1$ and $V_8$ on the Poincaré section. *Solid* and *dashed curves* are for $V_1$ and $V_8$, respectively

## Markov chain model

The statistical properties of in-out intermittency can be described by the Markov chain model (Ashwin et al. 1999). The Markov chain model for this intermittecy is schematically shown in Fig. 8. This model consists of two semi-infinite chains of states $p_i$ and $q_i$ representing *in-phase* and *out-phase*, respectively. Being in a state $p_i$ implies that the system are near the $SMW^{+-}$ which is transversely attracting; $q_i$ implies that it is near the *AS* state which is transversely repelling. The index $i$ corresponds to the distance from the mirror symmetric invariant subspace; the larger the value of $i$, the smaller is the distance from the invariant subspace. Since both of the *in-phase* and *out-phase* are periodic, only one-way transitions are allowed in both the *in-chain* $p_i$ and the *out-chain* $q_i$. The probability of the transitions $p_{i-1} \rightarrow p_i$ is denoted by $\alpha_D$. The probability of the transitions $p_i \rightarrow q_i$ is denoted by $\varepsilon$. Transitions $q_i \rightarrow q_{i-1}$ occur with probability 1.

By using this model, we can investigate the asymptotic behavior of the probability distributions of the duration of laminar phases in this intermittency $P(n)$, where $n$ is the laminar length. Details of the method are described in Ashwin et al. (1999). We have $P(n) \sim \varepsilon\,(1-\varepsilon)^n$ for large $n$. This distribution has exponential fall. We also calculate $P(n)$ for the attractor shown in Fig. 6a. Figure 9 shows the calculated $P(n)$, which has exponential fall off for large $n$. The behavior of our calculated $P(n)$ for large $n$ is compatible with the predicted asymptotic behavior by the Markov chain model.

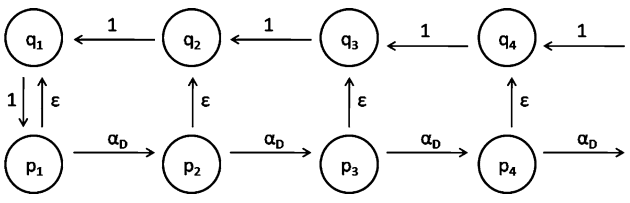


**Fig. 8** Schematic diagram showing transitions in the Markov model for the in-out intermittency. The probability of the transition $p_{i-1} \rightarrow p_i$ is denoted by $\alpha_D$. The probability of the transition $p_i \rightarrow q_i$ is denoted by $\varepsilon$

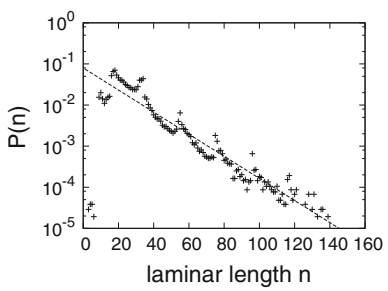


**Fig. 9** The probability distribution of the duration of laminar phases of the attractor shown in Fig. 6

### Bifurcations along with variation in the coupling strength

In the previous section, we discuss one of typical transitory behaviors. In this section, we show that the system exhibits further curious behaviors depending on $g$ ($g/N^2$).

Typical Poincaré maps in the range of $g/N^2 = 0.0008 \sim 0.0012$ are shown in descending order of $g/N^2$ in Fig. 10. These figures are in the case of $N = 33$.

In Fig. 10i, two fixed points and a string-like shaped attractor appear on the section. The fixed points represent stable periodic states on the $AMW_2^{\pm}$ branches shown in Fig. 3d. The $AMW_2^{\pm}$ branches are stable in the range of $g/N^2 = 0.00105 \sim 0.0013$. The largest Lyapunov exponent of string-like shaped attractor is small but still positive. Thus it is very weakly chaotic.

The weakly chaotic attractor disappears and only two fixed points survive in Fig. 10ii. The disappearance of this chaotic state results from a crisis occurring via the contact of chaotic trajectories with a stable manifold of the $SMW^{+-}$ state. Then this crisis is a boundary crisis (Grebogi et al. 1982). In Fig. 10iii, the $AMW_2^{\pm}$ states loose stability and then two tori appear instead.

In Fig. 10iv, the attractor in an eight-shaped fashion is shown. It is made by merging of the two tori in Fig. 10iii. This attractor is the same as the one discussed in "Transitory behaviors" except the absence of the weakly chaotic state. It is not a quasi-periodic attractor but a chaotic one, in which either of the two dynamical paths $MAMW_2^{\pm}$ from the $AS$ to the $SMW^{+-}$ is selected, not regularly but irregularly. This can also be interpreted as a kind of in-out intermittency. The distribution of the duration of laminar phases for this chaotic attractor obeys an exponential law for large $n$, as with the one for the attractor discussed in the previous subsection. Decrease in the coupling strength to $g/N^2 \sim 0.00094$ makes this chaotic attractor change into a quasi-periodic, although its Poincaré map looks almost the same as the one shown in Fig. 10iv. Nevertheless, the selection of the dynamical paths from $AS$ to $SMW^{+-}$ is regular in it.

In Fig. 10v, the weakly chaotic attractor which do not appear in Fig. 10ii–iv reappears as a dynamic component of the attractor discussed in the previous subsection. Even in the region characterized by the Poincaré sections shown in Fig. 10ii–iv, this chaotic state exists as a transient state. Once a trajectory visits the transient state, it finally goes to either of the fixed points, tori, or eight-shaped attractor depending on the coupling strength. Here, nevertheless, a collision between an stable manifold of $SMW^{+-}$ and the eight-shaped attractor occurs, and consequently a gateway to the weakly chaotic state in the vicinity of $SMW^{+-}$ is yielded. Thus, a trajectory can visit the weakly chaotic state over and over. This crisis is interior crisis (Grebogi et al. 1982), since it causes growth of the attractor size.

On the Poincaré section in Fig. 10vi, randomly scattered points appear in addition to an ordered structure similar to the one appearing in Fig. 10v. These randomly scattered points correspond to strong chaos. Spatio-temporal patterns corresponding to this Poincaré section consist of the patterns as shown in Fig. 5, turbulent patterns corresponding to the strong chaos, and spontaneous transitions among them (Tsuda et al. 2004). Such transitions can be interpreted as chaotic itinerancy (Tsuda et al. 2004; Ikeda et al. 1989; Kaneko 1990; Tsuda 1991, 1992; Kaneko and Tsuda 2003). In Fig. 10vii the ordered structure disappears and there remains strong chaos.

To specify the regions of $g/N^2$ characterized by such Poincaré maps as is shown in Fig. 10i–vii, we introduce useful quantities: The maximum and minimum Euclidean distances between the $AS$ state and current trajectory are measured on the Poincaré section, $d_{AS}^{max}$ and $d_{AS}^{min}$. Figure 11a, b show plots of $d_{AS}^{max}/\sqrt{N}$ and $d_{AS}^{min}/\sqrt{N}$ as a function of $g/N^2$ for $N = 16$, 20, 32, and 33. From these two figures, we clearly observe seven ranges of $g/N^2$. In these seven regions labeled i–vii, types of the Poincaré map shown in Fig. 10i–vii are obtained. Realization of the scaling mentioned in the "Bifurcation structures of periodic states and system size dependence" appears also in this figure: plots for different $N$ are almost independent of $N$. The scaling is sufficient for $N \geq 32$. Furthermore, it is seen that even for $N = 16$ the bifurcation structure is the same as the one for $N \geq 32$, though the scaling is not sufficient.

## Summary and discussion

We studied transitory behaviors in the population of diffusively interacting nonlinear oscillators which includes following synchrony in the case of two-oscillator system: the two oscillators synchronize in out-of-phase in the case of weak couplings, whereas, in the case of relatively strong couplings, they synchronize in in-phase or in anti-phase, depending on the initial condition. Large populations of such oscillators interacting via one-dimensional nearest neighbor couplings exhibit a variety of dynamical behaviors depending on the rescaled coupling strength. Among others, of special interest is the transitory behavior which consists of some sorts of metachronal waves, the all-synchronized state, and weakly chaotic state. We showed that it can be interpreted as in-out intermittency where the trajectory leaves and approaches the invariant subspace which stems from the mirror symmetry. Two saddles exist on the invariant subspace, which represent the

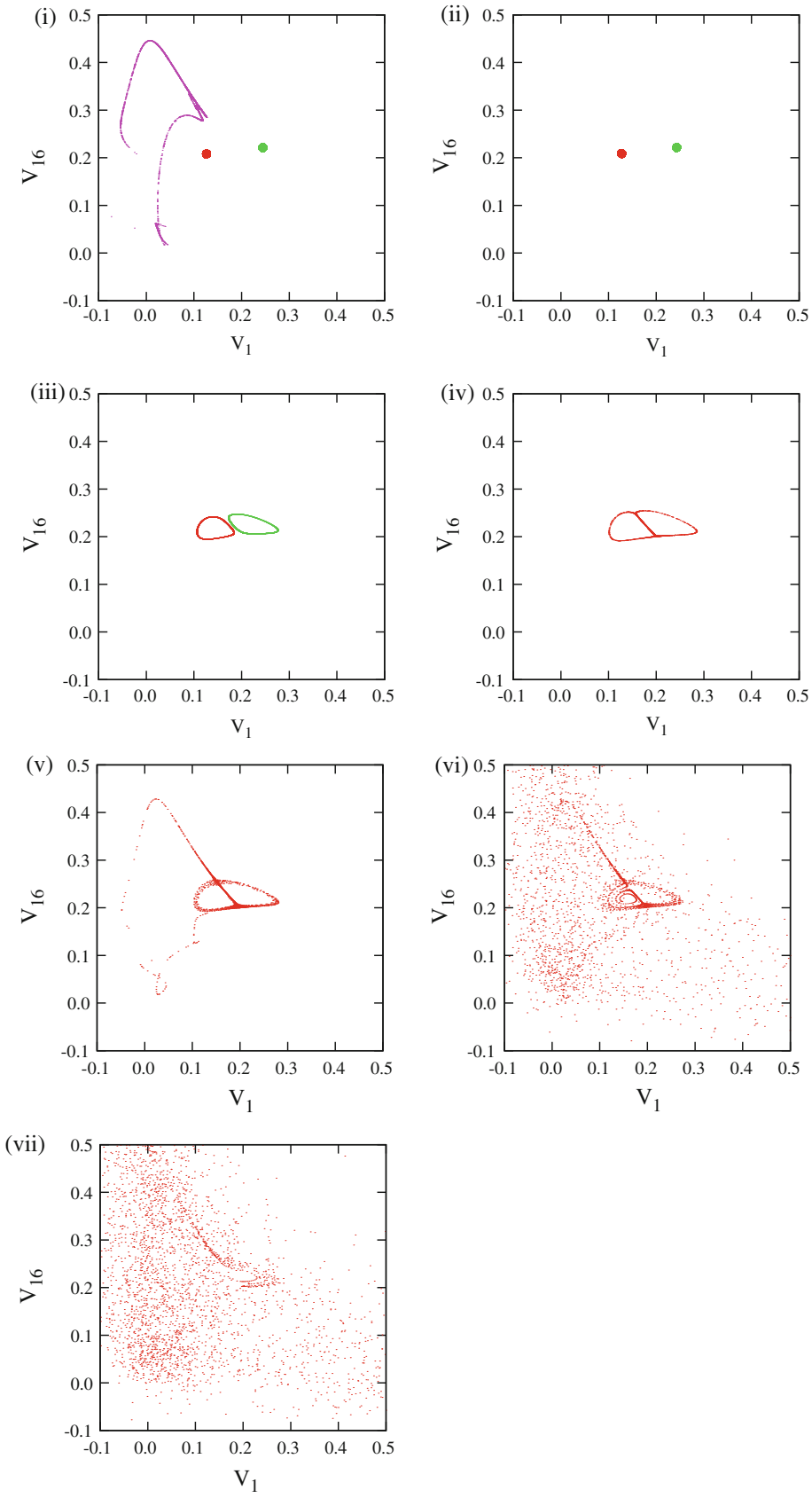


**Fig. 10** Typical Poincaré sections in the region of $g/N^2 = 0.0008$–$0.0012$. $N = 33$. **i** $g/N^2 = 0.00119$ ($g = 1.29591$). Two fixed points representing periodic states and a weakly chaotic attractor. **ii** $g/N^2 = 0.001175$ ($g = 1.279575$). Two fixed points. **iii** $g/N^2 = 0.001045$ ($g = 1.138005$). Two tori. **iv** $g/N^2 = 0.00103$ ($g = 1.12167$). An eight-shaped attractor. **v** $g/N^2 = 0.000975$ ($g = 1.061775$). The in-out intermittency discussed in the previous section. **vi** $g/N^2 = 0.00093$ ($g = 1.012770$). Intermittent transitions between the attractor ruin and the strong chaos. **vii** $g/N^2 = 0.0009$ ($g = 0.9801$). Strong chaos

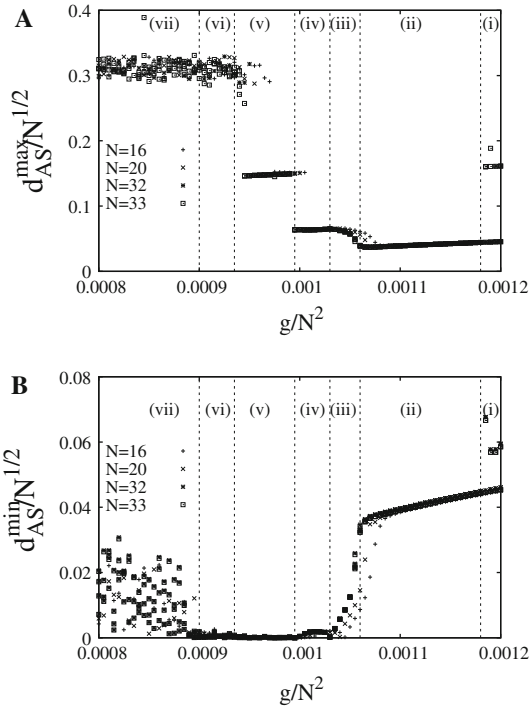


**Fig. 11** The quantities $d_{AS}^{max}/\sqrt{N}$ (**a**) and $d_{AS}^{min}/\sqrt{N}$ (**b**) as a function of $g/N^2$. Transient trajectories are omitted. The plots do not depend on the initial values of ($V_i$, $R_i$). In the regions marked with labels i–vii, types of the Poincaré sections i–vii shown in Fig. 10 appear, respectively

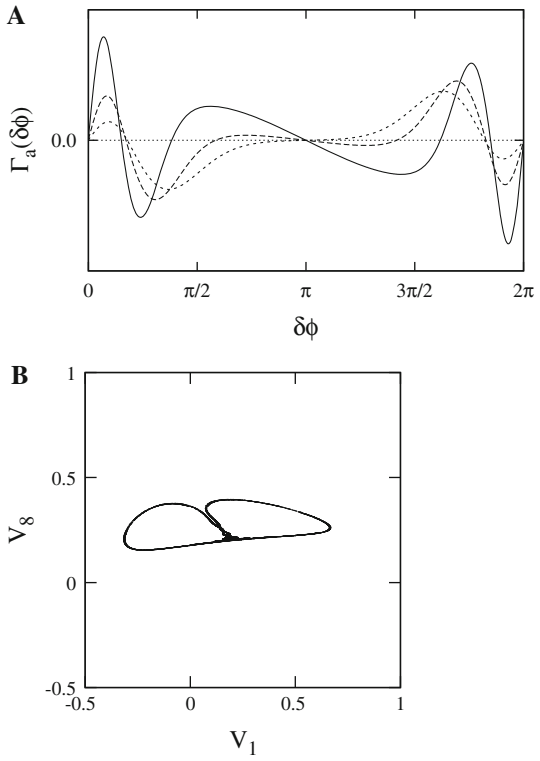


**Fig. 12** **a** Antisymmetric part of effective coupling for the two-dimensional Hindmarsh-Rose neuron (Hindmarsh and Rose 1984). *Solid*, *dashed*, and *dotted curves* are for $I = 0.20$, $I = 0.5$, and $I = 0.9$, respectively. **b** A Poincaré map for a diffusively coupled system of the Hindmarsh-Rose neurons. $N = 16$, $I = 0.20$, $g = 9.8$. The same hyperplane as in the case of the $\mu$-model is used as a Poincaré section

all-synchronized state and the symmetric metachronal wave. Because of their stabilities in the normal direction to the invariant subspace, the former and the latter give rise to the motion of leaving and approaching the invariant subspace, respectively.

Since connections between the two saddles are formed in the transitory behavior discussed here, it seems to be similar to the heteroclinic cycle. Nevertheless the staying periods in the neighborhood of the saddles in the behavior do not become infinite. Thus the behavior is a phenomenon different from the heteroclinic cycle.

Also in the case of some types of oscillator systems such as the Morris-Lecar model, which exhibit anti-phase synchrony in the weak coupling limit, their coupled systems can exhibit transitory behaviors, i.e. alternations between synchronization and desynchronization of oscillations (Han et al. 1995, 1997; Karantonis and Nakabayashi 2001; Han and Postnov 2003). Let us compare the transitory behaviors in the present study with the ones in the case of anti-phase synchronous oscillators. While transitory behaviors in Han et al. (1995, 1997), Karantonis and Nakabayashi (2001) can appear even in the case of $N = 2$ (Han and Postnov 2003), the transitory behaviors in the present model cannot appear. Because, one of the two saddles in the mirror symmetric invariant subspace, i.e. the $SMW^{+-}$ state, that is prerequisite for the transitory behavior in the present model, cannot exist in the case of $N = 2$. Thus transitory behaviors in the present study are essentially different from the ones in the case of anti-synchronous oscillators.

Are there any other oscillator systems exhibiting behaviors similar to the ones in the present study? The two-dimensional Hindmarsh-Rose neuron model (Hindmarsh and Rose 1984) exhibits out-of-phase synchrony in the weak coupling case like the $\mu$-model (see Fig. 12a). Their diffusively coupled system can exhibit similar transitory behaviors. A Poincaré map of one of such behaviors is shown in Fig. 12b, in which an attractor similar to the one in Fig. 10iv appears. This attractor also consists of the all-synchronized state and metachronal waves. It should be noted that all out-of-phase oscillator systems do not always exhibit transitory behaviors mentioned above when diffusively coupled. The conditions for the appearance of the transitory behaviors described here are in the future study.

In the present paper, the case of one-dimensional nearest neighbor coupling is discussed. We further investigated $N \times N$ oscillators interacting via the two-dimensional nearest neighbor coupling. We also found that such

coupled systems exhibit various transitory behaviors (not shown here) in the regions of $g(g/N^2)$ and $I$ where the all-synchronized state becomes a saddle. We will report these issues, elsewhere.

## References


Ashwin P, Cova E, Tavakol R (1999) Transverse instability for non-normal parameters. Nonlinearity 12:563–577

Benettin G, Galgani L, Giorsilli A, Strelcyn JM (1980a) Lyapunov characteristic exponents for smooth dynamical systems and for hamiltonian systems; a method for computing all of them part 1: theory. Mecannica 15:9–20

Benettin G, Galgani L, Giorsilli A, Strelcyn JM (1980b) Lyapunov characteristic exponents for smooth dynamical systems and for hamiltonian systems; a method for computing all of them part 2: numerical application. Mecannica 15:21–30

Doedel EJ, Paffenroth RC, Champneys A, Fairgrieve T, Kuznetsov Y, Oldeman B, Sandstede B, Wang X (2002) Auto2000: continuation and bifurcation software for ordinary differential equations with homcont. http://cmvl.cs.concordia.ca/auto

Fujii H, Tsuda I (2004) Neocortical gap junction-coupled interneuron systems may induce chaotic behavior itinerant among quasi-attractors exhibiting transient synchrony. Neurocomputing 58–60:151–157

Galarreta M, Hestrin S (1999) A network of fast-spiking cells in the neocortex connected by electrical synapses. Nature 402:72–75

Gibson JR, Beierlein M, Connors BW (1999) Two networks of electrically coupled inhibitory neurons in neocortex. Nature 402:75–79

Gray CM, Koenig P, Engel AK, Singer WO (1992) Synchronization of oscillatory neuronal responses in cat striate cortex: temporal properties. Vis Neurosci 8:337–347

Grebogi C, Ott E, Yorke JA (1982) Chaotic attractors in crisis. Phys Rev Lett 48:1507–1510

Han SK, Postnov DE (2003) Chaotic bursting as chaotic itinerancy in coupled neural oscillators. Chaos 13:1105–1109

Han SK, Kurrer C, Kuramoto Y (1995) Dephasing and bursting in coupled neural oscillators. Phys Rev Lett 75:3190–3193

Han SK, Kurrer C, Kuramoto Y (1997) Diffusive interaction leading to dephasing of coupled neural oscillators. Int J Bifurcat Chaos 7:869–875

Hindmarsh JL, Rose RM (1984) A model of neuronal bursting using three coupled first order differential equations. Proc R Soc B 221:87–102

Ikeda K, Otsuka K, Matsumoto K (1989) Maxwell-bloch turbulence. Prog Theor Phys Suppl 99:295–324

Kaneko K (1990) Clustering, coding, switching, hierarchical ordering, and control in network of chaotic elements. Phys D 41:137–172

Kaneko K, Tsuda I (eds) (2003) Chaotic itinerancy. Focus issue in chaos 13:926–1164

Karantonis A, Nakabayashi S (2001) Phase flow deformations and coupled electrochemical oscillators. Chem Phys Lett 347: 133–137

Kenet T, Bibitchkov D, Tsodyks M, Grinvald A, Arieli A (2003) Spontaneously emerging cortical representations of visual attributes. Nature 425:954–956

Kuramoto Y (1984) Chemical oscillations, waves, and turbulence. Spinger, Berlin

Sherman A, Rinzel J (1992) Rhythmogenetic effects of weak electrotonic coupling in neuronal models. Proc Natl Acad Sci USA 89:2471–2474

Shimada I, Nagashima T (1979) A numerical approach to ergodic problem of dissipative dynamical systems. Prog Theor Phys 68:349–358

Tsuda I (1991) Chaotic itinerancy as a dynamical basis of hermeneutics in brain and mind. World Futures 32:167–184

Tsuda I (1992) Dynamic link of memories—chaotic memory map in nonequilibrium neural networks. Neural Netw 5:313–326

Tsuda I, Fujii H, Tadokoro S, Yasuoka T, Yamaguti Y (2004) Chaotic itinerancy as a mechanism of irregular changes between synchronization and desynchronization in a neural network. J Integr Neurosci 3:159–182